



ELSEVIER

Coastal Engineering 46 (2002) 291–313

**Coastal  
Engineering**  
An International Journal for Coastal,  
Harbour and Offshore Engineers

www.elsevier.com/locate/coastaleng

# Laboratory study of wave and turbulence characteristics in narrow-band irregular breaking waves

Francis C.K. Ting\*

*Department of Civil and Environmental Engineering, South Dakota State University, CEH 210, Box 2219, Brookings,  
SD 57007-0495, USA*

Received 15 January 2002; received in revised form 3 June 2002; accepted 28 June 2002

## Abstract

Wave elevations and water particle velocities were measured in a laboratory surf zone created by the breaking of a narrow-band irregular wave train on a 1/35 plane slope. The incident waves form wave groups that are strongly modulated. It is found that the waves that break close to the shoreline generally have larger wave-height-to-water-depth ratios before breaking than the waves that break farther offshore. After breaking, the wave-height-to-water-depth ratio for the individual waves approaches a constant value in the inner surf zone, while the standard deviation of the wave period increases as the still water depth decreases. In the outer surf zone, the distribution of the period-averaged turbulent kinetic energy is closely correlated to the initial wave heights, and has a wider variation for narrow-band waves than for broad-band waves. In the inner surf zone, the distribution of the period-averaged turbulent kinetic energy is similar for narrow-band waves and broad-band waves. It is found that the wave elevation and turbulent kinetic energy time histories for the individual waves in a wave group are qualitatively similar to those found in a spilling regular wave. The time-averaged transport of turbulent kinetic energy by the ensemble-averaged velocity and turbulence velocity under the irregular breaking waves are also consistent with the measurements obtained in regular breaking waves. The experimental results indicate that the shape of the incident wave spectrum has a significant effect on the temporal and spatial variability of wave breaking and the distribution of turbulent kinetic energy in the outer surf zone. In the inner surf zone, however, the distribution of turbulent kinetic energy is relatively insensitive to the shape of the incident wave spectrum, and the important parameters are the significant wave height and period of the incident waves, and the beach slope.

© 2002 Elsevier Science B.V. All rights reserved.

*Keywords:* Breaking waves; Surf zone; Irregular waves; Turbulent kinetic energy; Reynolds stress; Wave height distribution; Wave period distribution; Narrow-band spectrum; Wave groups; Plane beach

## 1. Introduction

For regular waves incident on a plane beach, the patterns of wave breaking depend primarily on the

incident wave height, wave period and beach slope. The four types of breakers that have been identified are spilling, plunging, collapsing and surging (Galvin, 1968; Goda, 1970). Battjes (1974) found that the different types of breakers can be characterized by the surf similarity parameter. When calculated based on the deep-water wave height  $H_0$  and wave

\* Tel.: +1-605-688-5997; fax: 1-605-688-5878.

E-mail address: francis\_ting@sdstate.edu (F.C.K. Ting).

length  $L_0$ , the surf similarity parameter is defined as

$$\xi_0 = \frac{\tan \beta}{\sqrt{H_0/L_0}} \quad (1)$$

where  $\tan \beta$  is the beach slope. The following regimes were found from Galvin's experimental data:

$$\begin{aligned} \xi_0 < 0.5 & \quad (\text{spilling breakers}) \\ 0.5 < \xi_0 < 3.3 & \quad (\text{plunging breakers}) \\ \xi_0 > 3.3 & \quad (\text{surging breakers}) \end{aligned} \quad (2)$$

The turbulent flow fields associated with spilling and plunging breakers are of fundamental importance to the dynamic equilibrium of beaches (Dean, 1973; Dalrymple, 1992), and have been studied extensively both in the laboratory (Stive, 1980; Stive and Wind, 1982; Nadaoka and Kondoh, 1982; Okayasu et al., 1986; Nadaoka et al., 1989; Ting and Kirby, 1995, 1996; Cox et al., 1996; Cox and Kobayashi, 2000) and by computer simulations (Deigaard et al., 1986; Lemos, 1992; Lin and Liu, 1998a,b; Bradford, 2000). These studies have generated a detailed picture of the breaking and decay of regular waves in a laboratory surf zone, and of the generation and evolution of the related turbulent flow fields.

For irregular waves, the relationships between incident wave characteristics and wave breaking patterns are not clearly understood. If the beach slope is held constant, then the temporal and spatial variability of wave breaking should depend only on the characteristics of the incident wave spectrum. In shallow water, the TMA spectrum (Bouws et al., 1985) is widely used by coastal engineers. The TMA spectrum is specified by the spectral significant wave height  $H_{m0}$ , spectral peak wave period  $T_p$ , water depth  $h$ , and the spectra shape parameters  $\alpha$ ,  $\gamma$  and  $\sigma$ . Therefore, it is expected that the wave breaking patterns should also depend on these parameters.

Sultan (1995) measured the water particle velocities under irregular breaking waves on a plane beach using a two-component laser Doppler anemometer. To define a surf similarity parameter for irregular waves, he calculated  $H_0$  by taking the spectral significant wave height in the horizontal portion of the wave tank

and backing it out to deep water as if it were a monochromatic wave with period  $T_p$ , and defined  $L_0$  as the deep-water wave length associated with  $T_p$ . Three wave conditions ( $\xi_0 = 0.16, 0.37$  and  $0.66$ ) were studied in the laboratory experiments. The three wave conditions provided one wave time series with predominantly spilling breakers, one with predominantly plunging breakers, and one in between. Several features found in regular waves were observed in the irregular waves. For example, the "plunging" wave condition has a narrower surf zone and steeper wave set-up than the other two wave conditions. The "plunging" wave condition has a larger wave-height-to-water-depth ratio in the inner surf zone than the "spilling" wave condition. The correlation between the ensemble-averaged velocity and turbulent kinetic energy is negative (seaward) for the "spilling" wave condition, and positive (landward) for the "plunging" wave condition. In general, it was found that the effect of wave irregularity is to reduce the distinctiveness of features that are reported for regular waves. Unlike regular breaking waves, which may be classified into one of the four categories described earlier, the irregular breaking waves in Sultan's experiments were a mix of spilling, plunging and non-breaking waves.

The "spilling" and "plunging" wave conditions in Sultan (1995) have the same spectra shape, but different significant wave heights and periods. The present study, however, is concerned with a narrow-band wave spectrum. The frequency content of the incident waves is concentrated over a very narrow range. The interaction of waves of slightly different frequencies produces wave groups that are strongly modulated. The motivation for this study is to examine the effects of spectra shape on the wave and turbulence characteristics inside the surf zone.

In a recent study, Svendsen and Veeramony (2001) conducted wave measurements with periodic wave groups incident on a plane beach. Each wave group was composed of five cnoidal waves, all with the same period but with varying heights. Since shallow water waves are nearly nondispersive, and the group and phase velocities are equal, the waves in the wave groups remained distinct as they travelled from gage to gage. Svendsen and Veeramony (2001) found that the location of the start of breaking of the individual waves in a group is closely correlated with the initial

variation of wave heights within the group. The breaking of the narrow-band waves described in this article follows a similar pattern. However, our emphasis is on the fluid kinematics under the wave groups. The velocity measurements are related to the wave transformation through the surf zone, and comparisons are made with experimental data from other wave conditions to shed light on the effects of the shape of the incident wave spectrum on the turbulence characteristics inside the surf zone.

## 2. Experimental procedure

In this section a brief account of the experimental equipment and procedure will be presented. For a detailed description, the interested reader is referred to Ting (2001).

The experiment was conducted in a 37-m-long, 0.91-m-wide and 1.22-m-deep glass-walled wave flume equipped with a hinged-flap programmable wave maker. A 1 on 35 sloped false bottom built of marine plywood was installed in this tank to create a plane beach. The still water depth at the toe of the beach was 45.72 cm (Fig. 1).

One wave time series was used in all the test runs. The duration of wave generation was 10 min. Excellent repeatability was observed for different runs of the same time series (Sultan and Ting, 1993; Ting, 2001). Fig. 2 shows the wave spectrum measured in the horizontal portion of the wave tank. The incident waves were developed from the TMA spectrum, with the following parameter values:  $H_{m0} = 0.1229$  m,

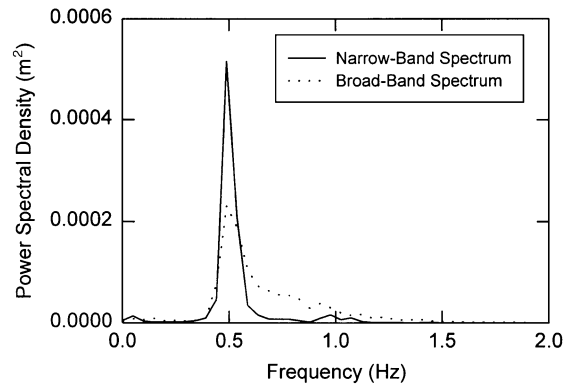


Fig. 2. Measured wave spectrum in the horizontal portion of the wave tank. The entire wave record of 5.12 min is divided into 15 equal segments. Each segment is separately FFT'd and the resulting power spectral density estimates are averaged at each frequency in the Nyquist frequency range.

$T_p = 2.0$  s,  $\gamma = 100$ ,  $\sigma = 0.07$  (for  $f < f_p$ ) and 0.09 (for  $f > f_p$ ), where  $f_p$  is the frequency of the spectral peak. The corresponding value of  $\xi_0$  is 0.20. Also plotted in Fig. 2 is a broad-band spectrum (Ting, 2001). The assigned values of  $H_{m0}$ ,  $T_p$  and  $\gamma$  for the broad-band spectrum are 0.1524 m, 2.0 s and 3.3, respectively, and the corresponding value of  $\xi_0$  is 0.18. Note that increasing the value of  $\gamma$  produces the narrow-band spectrum. For both wave spectra, wave breaking on the beach was dominated by spilling breakers. A notable difference between the two wave conditions is that the incident waves from the narrow-band spectrum are strongly modulated, whereas the incident waves from the broad-band spectrum are more or less random.

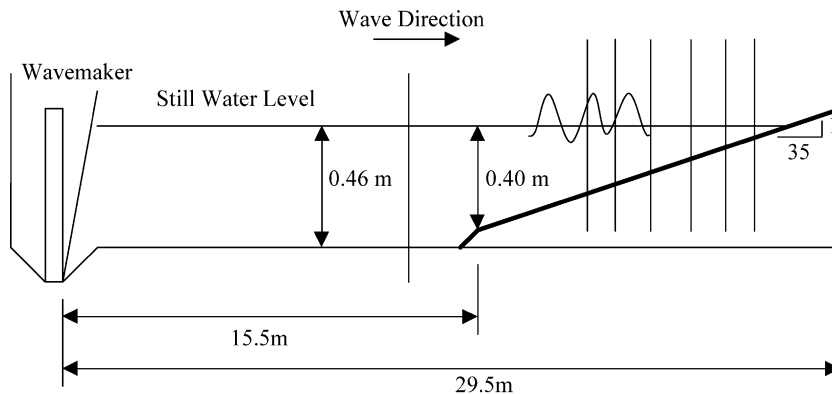


Fig. 1. Experimental arrangement. The wave gage positions are shown as vertical lines.

Table 1  
Summary of measured wave statistics

$d$ (cm)	45.72	27.04	22.77	18.23	13.72	9.39	6.25
$\bar{\zeta}$ (cm)	0.0	0.0	0.0	0.0	-0.03	0.33	0.58
$h$ (cm)	45.72	27.04	22.77	18.23	13.69	9.72	6.83
$h/H_0$	3.62	2.14	1.80	1.44	1.08	0.77	0.54
$H_{\max}$ (cm)	14.82	19.90	18.75	17.17	13.38	10.43	6.78
$H_{1/10}$ (cm)	13.70	18.05	17.52	15.99	11.82	8.65	5.19
$H_{1/3}$ (cm)	12.16	15.79	15.77	14.07	10.17	7.12	4.47
$H_{\text{rms}}$ (cm)	8.92	11.33	11.39	10.36	7.99	5.73	3.58
$H_{\text{mean}}$ (cm)	8.19	10.26	10.36	9.44	7.62	5.49	3.42
$T_{\max}$ (s)	1.90	1.88	2.06	1.82	1.78	2.99	1.19
$T_{1/10}$ (s)	1.94	2.00	2.00	1.99	1.91	1.83	2.07
$T_{1/3}$ (s)	1.98	1.98	2.00	1.98	1.92	1.90	2.02
$T_{\text{mean}}$ (s)	1.95	1.98	1.97	1.90	1.95	1.91	1.89
Number of waves	157	154	154	161	156	160	162
Percent breaking	0	2	10	31	63	82	96

$d$ =still water depth;  $\bar{\zeta}$ =wave set-up;  $h$ =mean water depth;  $H_0$ =deep-water significant wave height;  $H_{\max}$ =wave height of the highest wave;  $H_{1/10}$ =average wave height of the highest one-tenth wave;  $H_{1/3}$ =average wave height of the highest one-third wave;  $H_{\text{rms}}$ =root-mean-square wave height;  $H_{\text{mean}}$ =mean wave height;  $T_{\max}$ =wave period of the highest wave;  $T_{1/10}$ =average wave period of the highest one-tenth wave;  $T_{1/3}$ =average wave period of the highest one-third wave;  $T_{\text{mean}}$ =mean wave period.

Water surface elevations were measured in the horizontal portion of the wave tank and at six locations on the plane beach sequentially using a resistance-type gage. The wave gages were in water depths of 45.72, 27.04, 22.77, 18.23, 13.72, 9.39 and 6.25 cm. The gage positions are shown as vertical lines in Fig. 1. A summary of the measured wave statistics is given in Table 1. At  $d=13.72$ , 9.39 and 6.25 cm, 10 wave time series obtained under the same experimental conditions were used to establish an ensemble-

averaged wave time series for each location, and wave statistics were computed on the ensemble averages.

Water particle velocities were measured at three cross-shore locations inside the surf zone; the locations of velocity measurements are given in Table 2. At each location, the longitudinal and vertical velocity components were measured using a laser Doppler anemometer (LDA) simultaneously with the wave elevation. The LDA is a backscatter, three-beam system built by Dantec Electronics. It consists of a 4-W argon-ion laser (Innova 70-5 from Coherent), transmitting and receiving optics, traverse mechanism, and one frequency tracker and shifter for each velocity component. The optics were mounted outside the wave tank and only the laser beams entered the water. The beam crossing point was 180 mm from the inside surface of the glass side wall. Titanium dioxide particles were used to “seed” the wave tank to provide tracer particles for scattering the laser light. For improved accuracy, the frequency trackers were calibrated using a polynomial fit between the input frequency from a frequency generator and the analog voltage output. The uncertainty in velocity measurements was  $\pm 0.5$  cm/s. Typical signal drop-out rate was 4% where the laser beams were never above the water surface.

At five measurement points (see Table 2), the experiment was repeated 10 times with the exact same incident wave time series. The average of all 10 runs represents an ensemble average. The sampling frequency was 100 Hz per channel. Data acquisition was synchronized with wave generation to start at the same time. Wave data and velocity data were collected for 8.192 min from the start of wave generation, but only the last 5.12 min of data were analyzed in order

Table 2  
Locations of velocity measurements

$d=13.72$ cm									
$z$ (cm)	-4.0	-5.0*	-6.0	-7.0	-8.0	-9.0	-10.0*	-11.0	-12.0
$(z-\bar{\zeta})/h$	-0.290	-0.363	-0.436	-0.509	-0.582	-0.655	-0.728	-0.801	-0.874
$d=9.39$ cm									
$z$ (cm)	-3.0	-4.0*	-5.0	-6.0*	-7.0	-7.5			
$(z-\bar{\zeta})/h$	-0.343	-0.446	-0.548	-0.651	-0.754	-0.806			
$d=6.25$ cm									
$z$ (cm)	-2.0	-3.0	-4.0*	-4.9					
$(z-\bar{\zeta})/h$	-0.378	-0.524	-0.671	-0.802					

The locations where wave velocities were measured by ensemble averaging are indicated by an asterisk. The still water level is located at  $z=0$ .

to minimize transient effects. Approximately 15 min was allowed between each test run to allow the long waves in the tank to dissipate.

Long waves were generated by wave breaking and re-reflected from the wave maker. Because of this, the wave climate in the wave tank was different from that on a natural beach where the reflected long waves would just go out to sea. It is impossible to generate irregular waves in a wave tank without the re-reflected long waves. The approach taken in this study is to provide as much information on the long-wave motion as possible so that one may account for long-wave noise in the data.

To reduce the effect whereby small waves riding on long waves may be carried entirely above or below the

mean water level, the long waves were filtered out before computing the wave height and period of the short waves. The filtering was done by a Fourier filter at a cutoff frequency of 0.2 Hz. Individual waves in the short-wave and long-wave time series were defined using the zero-downcrossing method. The measured instantaneous velocities were partitioned into a low-pass and a high-pass time series in the same manner as the wave elevations. The ensemble average of the low-pass velocity time series consists of the undertow and the long-wave velocity. The ensemble average of the high-pass velocity time series is the short-wave velocity. The difference between the high-pass velocity time series and the short-wave velocity is defined as the turbulent velocity fluctuation.

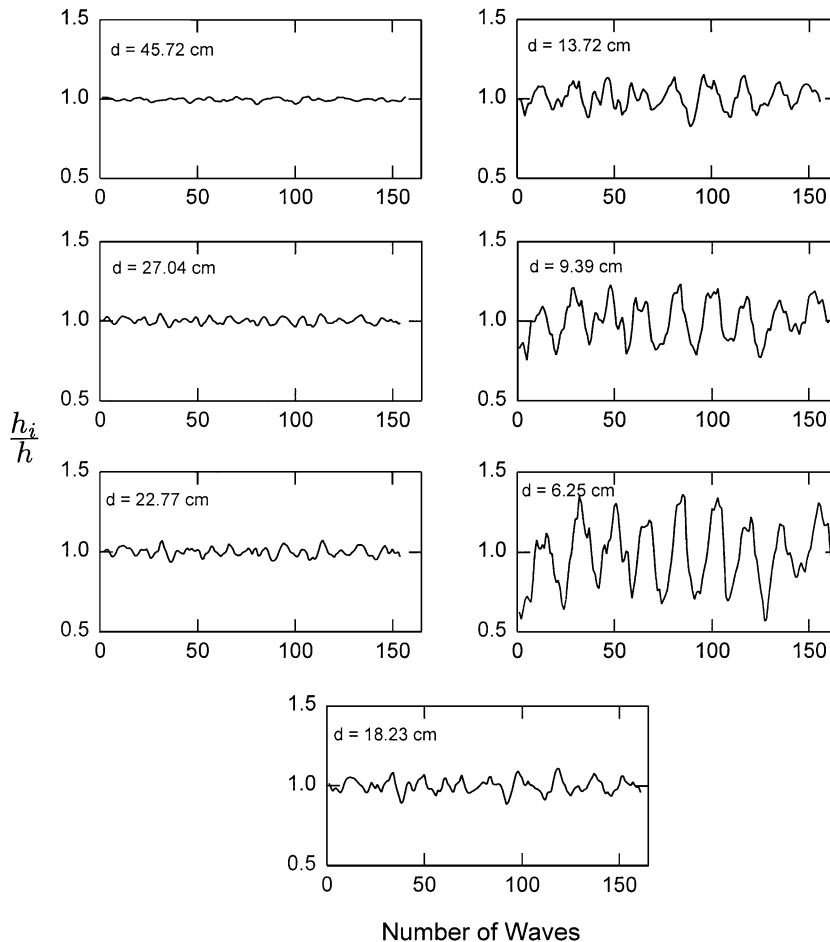


Fig. 3. Ratio of short-wave-averaged water depth to time-averaged water depth.

In addition to the velocity and wave elevation measurements, a video camera was used to record the surface waves at each wave gage position on the beach. The video records were examined to determine the locations of wave breaking and the breaker types.

### 3. Results and discussion

#### 3.1. Wave characteristics

To determine the time-varying water depth associated with the long-wave motion, the low-pass wave time series was averaged over the wave period of the individual short waves and added to the still water

depth. Fig. 3 is a plot of the period-averaged water depth,  $h_i$  ( $i = 1, \dots, N$ ), where  $N$  is the total number of short waves in the wave record. Note that  $h_i$  has been normalized by  $h$ , the time-averaged water depth. Fig. 3 shows that the period-averaged water depth varies considerably from wave to wave as the still water depth decreases. At  $d = 6.25$  cm, the last wave gage position near the shoreline, the  $h_i/h$  ratio ranges from 0.57 to 1.36. The long-wave motion has a significant effect on the short waves; this will be discussed.

Fig. 4 is a plot of the short-wave height,  $H_i$ , normalized by the period-averaged water depth,  $h_i$  ( $i = 1, \dots, N$ ). The incident waves form wave groups that are strongly modulated (i.e. large variation in wave height). The  $H_i/h_i$  ratio for the individual waves

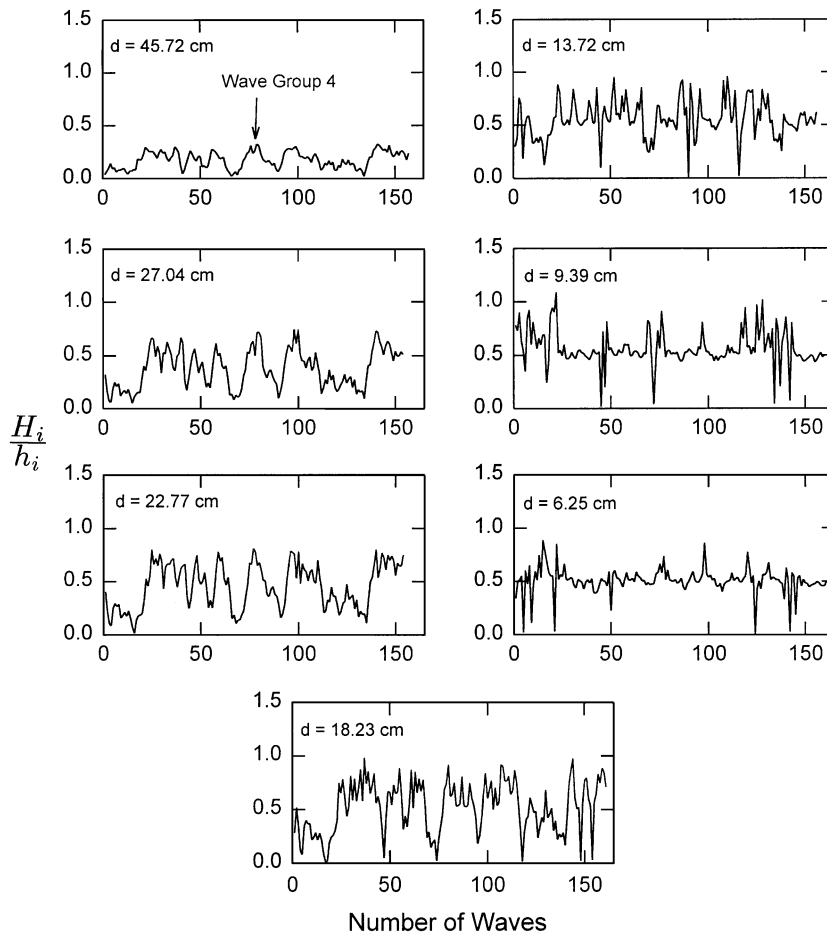


Fig. 4. Wave-height-to-water-depth ratio for short waves.

increases to a maximum value of 0.7 to 1.1 before wave breaking, and then decreases steadily to a constant value of about 0.5 inside the surf zone. Similar wave-height-to-water-depth ratios have been observed in spilling regular waves (e.g. Svendsen et al., 1978; Ting and Kirby, 1994). It is found that normalizing  $H_i$  by  $h_i$  produces a narrow variation in the  $H_i/h_i$  ratio for the broken waves. Fig. 4 also shows that the level of groupiness is greatly reduced inside the surf zone by the wave breaking process.

Fig. 4 shows that most of the waves have reached a depth-limited condition at  $d=6.25$  cm. This location is considered to be the beginning of the inner surf

zone. The surf zone seaward of this point is defined as the outer surf zone.

Fig. 5 is a plot of the short-wave period,  $T_i$  ( $i=1, \dots, N$ ), normalized by  $T_{1/3}$ . The latter is the average period of the highest one-third wave (the significant wave). This figure shows that the wave period has a narrow variation in the horizontal portion of the wave tank (the incident waves are narrow banded), but a much wider variation inside the surf zone. In addition, the variation of wave period has a period of about 40 s, which suggests that the wave period as well as the wave height of the short waves were affected by the long-wave motion.

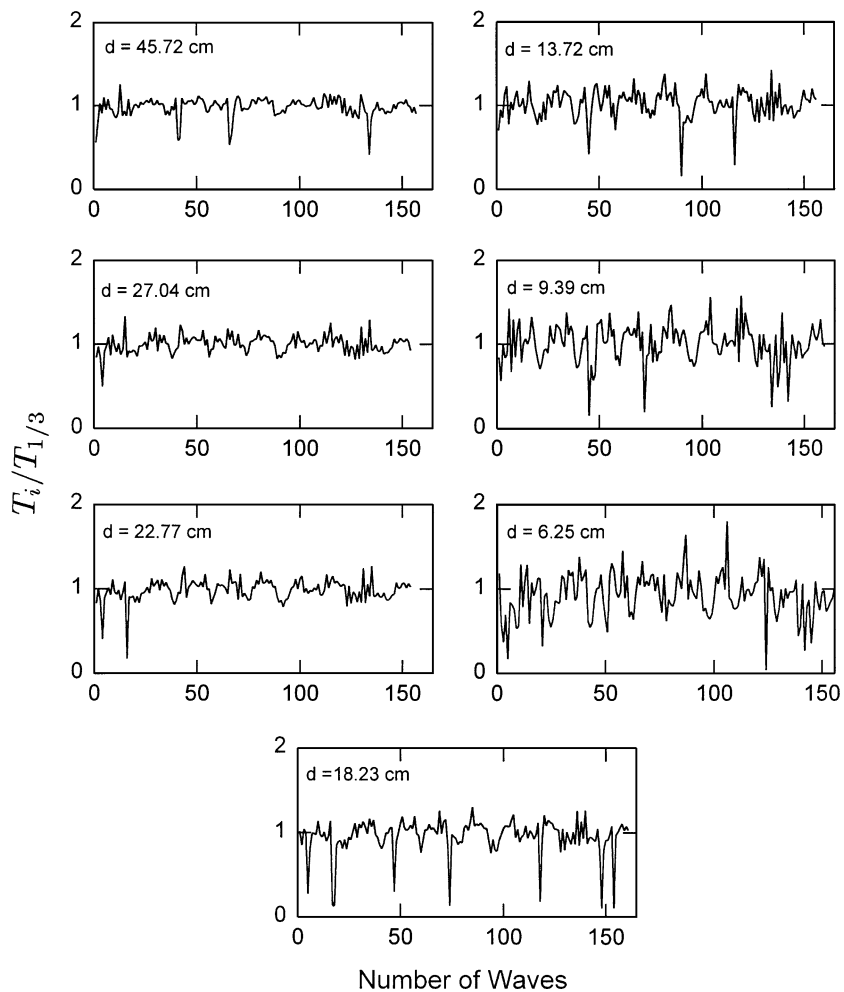


Fig. 5. Normalized wave period for short waves.

To understand the wave transformation through the surf zone better, Fig. 6 presents the variation of water surface profile with time for wave group 4 (see Fig. 4). Note that the short-wave elevation,  $\zeta_s$ , has been normalized by the time-varying water depth associated with the long-wave motion,  $\zeta_l + h$ . Wave group 4

is consisted of approximately 19 waves. It is strongly modulated, with high waves near the center and small waves at the head and rear of the group.

At  $d = 45.72$  cm, wave 19 is the smallest wave ( $H_i/h_i = 0.089$ ) in the group, and wave 9 is the largest ( $H_i/h_i = 0.327$ ); the ratio of the two wave heights is 0.27.

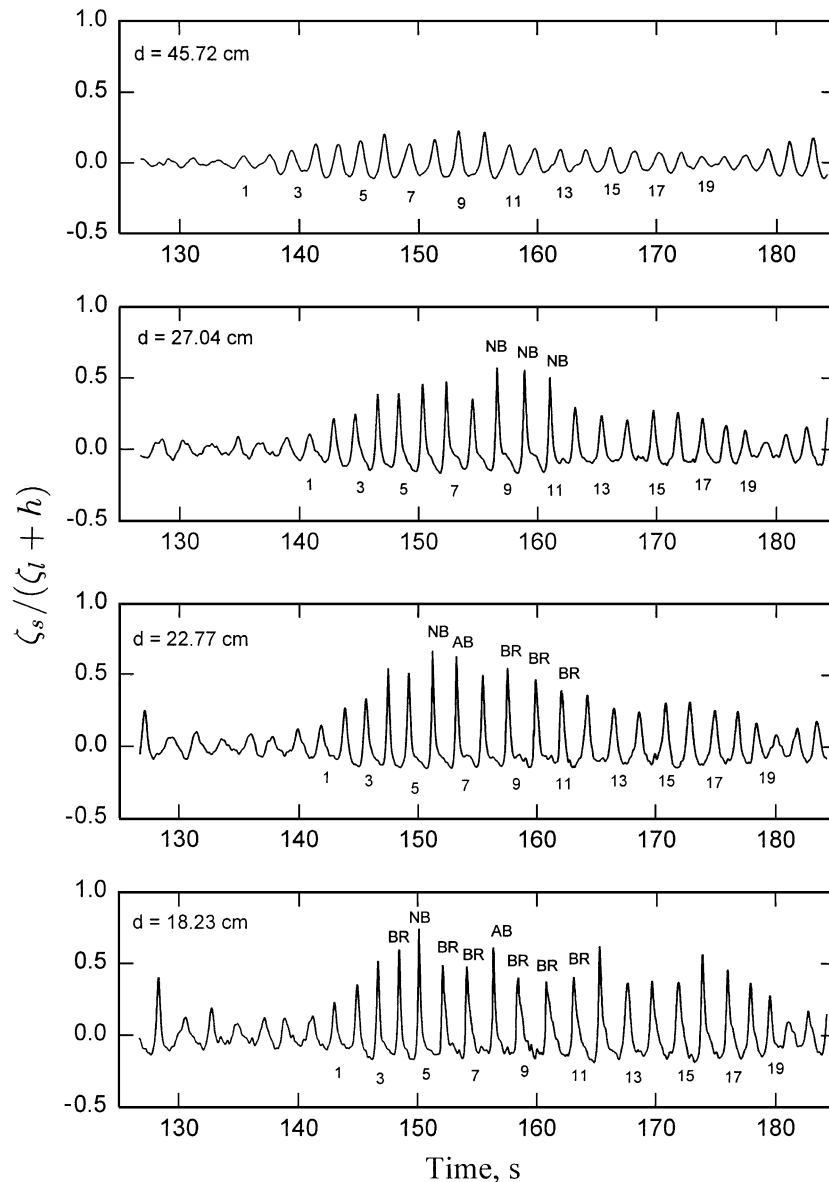


Fig. 6. Water surface elevation time series for wave group 4; NB—near breaking, B—breaking, AB—after breaking, and B—broken. The short-wave elevation has been normalized by the time-varying water depth associated with the long-wave motion.

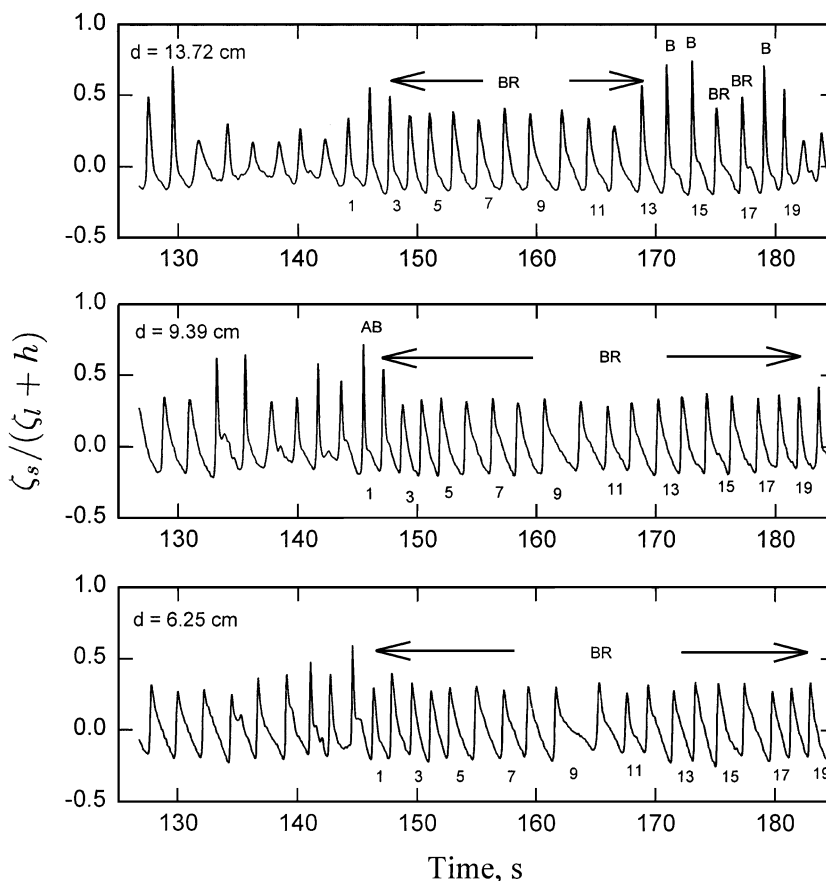


Fig. 6 (continued).

The  $H_i/h_i$  ratio for the individual waves increases as the still water depth decreases. At  $d=27.04$  cm, the three highest waves in the group (9, 10 and 11) are near breaking; wave breaking is defined to occur when air begins to be entrained at the wave crest. The values of  $H_i/h_i$  for waves 9, 10 and 11 are 0.718, 0.718 and 0.670, respectively. At  $d=22.77$  cm, waves 9, 10 and 11 have already broken. Wave 6, which is near breaking, has become the highest wave ( $H_i/h_i=0.812$ ) in the group. Breaking has just started for wave 7, the second highest wave ( $H_i/h_i=0.782$ ). The smallest wave in the group is wave 1 ( $H_i/h_i=0.229$ ).

At  $d=18.23$  cm, three more waves (4, 6 and 7) have broken. Wave 8 has just broken, and wave 5 is near breaking. The values of  $H_i/h_i$  for waves 5 and 8 are 0.915 and 0.749, respectively. Note that it is the

waves with the larger initial heights (4, 5, 6, 7, 8, 9, 10 and 11) that break first.

At  $d=13.72$  cm, three waves with the smaller initial heights (waves 3, 16 and 17) have broken. Waves 14, 15 and 18 are breaking. The values of  $H_i/h_i$  for waves 14, 15 and 18 are 0.894, 0.928 and 0.897, respectively. At  $d=9.39$  cm, all 19 waves in the group except wave 1 have broken. Wave breaking has just started for wave 1, and its value of  $H_i/h_i$  is 0.911.

At  $d=6.25$  cm, most of the broken waves have developed a sawtooth-shaped profile. The  $H_i/h_i$  ratio for the 19 waves has a narrow variation; the minimum value of  $H_i/h_i$  is 0.420, the maximum is 0.607, and the mean is 0.509.

Fig. 7 is a plot of the wave-height-to-water-depth ratio,  $H_i/h_i$ , versus the horizontal distance from the breaking point,  $(x - x_b)/h_b$ , for waves 9, 6, 5, 15 and 1.

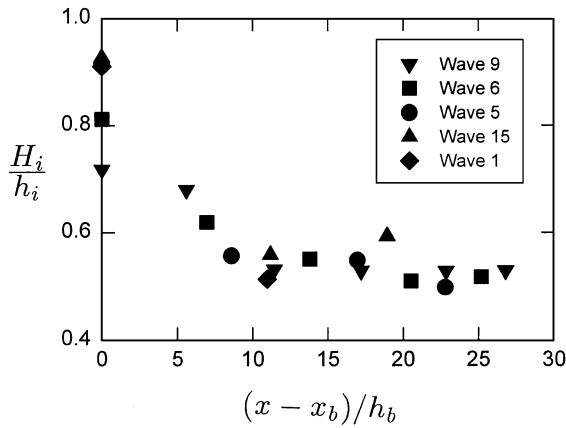


Fig. 7. Variation of wave-height-to-water-depth ratio with horizontal distance from the breaking point. The horizontal distance from the breaking point,  $x - x_b$ , has been normalized by the breaking depth,  $h_b$ .

The five waves are arranged in descending order of initial wave heights. These waves break at different positions ( $d=27.04$ ,  $22.77$ ,  $18.23$ ,  $13.72$  and  $9.39$  cm). The order in which the waves break follows their initial heights. Wave 9 breaks first, followed by waves 6, 5, 15 and then 1 (see Fig. 6). Fig. 7 shows that although wave 1 has the smallest initial height, it has one of the largest  $H_i/h_i$  ratio at breaking, whereas wave 9 has the largest initial height and the smallest  $H_i/h_i$  ratio at breaking. These results are consistent with regular wave breaking. It is well known for regular waves that the wave-height-to-water-depth ratio at breaking,  $H_b/h_b$ , increases as the deep-water wave steepness,  $H_0/L_0$ , decreases (e.g. when the breaker type changes from spilling to plunging). Furthermore, small waves would break closer to shore than large waves.

Fig. 6 shows that the wave period has a narrow variation in the horizontal portion of the wave tank. At  $d=45.72$  cm, wave 18 is the shortest wave ( $T_i=1.74$  s) in the wave group, and wave 14 is the longest ( $T_i=2.20$  s). The range of wave period increases as the still water depth decreases. At  $d=6.25$  cm, wave 1 has the smallest wave period (1.25 s), and wave 10 the largest (3.31 s). It may be observed in Fig. 6 that the wave period for waves 1, 13, 14 and 15 has decreased, while the period for waves 9 and 10 has increased considerably.

The up-shifting and down-shifting in wave period are related to variations in the phase velocity of the

waves in the wave groups. The wave gages were positioned too far apart to accurately measure the phase velocity at each gage. Therefore, the phase velocity was computed as follows:  $C_1=(gh)^{1/2}$ ,  $C_2=(gh_i)^{1/2}$ ,  $C_3=[gh_i(1+H_i/h_i)]^{1/2}$  and  $C_4=[gh_i(1+H_i/h_i)]^{1/2}+U_i$ , to investigate the effects of time-varying water depth, wave height variation and orbital velocity of the long waves on the phase velocity. Here,  $h$  is the time-averaged water depth,  $h_i$  is the period-averaged water depth,  $H_i$  is the short-wave height, and  $U_i$  is the longitudinal velocity of the long waves averaged over the period of the short waves. The computed results are plotted in Fig. 8.

As shown in Fig. 8, the time-varying water depth resulting from the long-wave motion has a significant effect on the phase velocity of the short waves. Comparing the phase velocity calculated using the time-varying water depth,  $C_2$ , to that calculated using the time-averaged water depth,  $C_1$ , the phase velocity is increased for waves 4 through 9, and decreased for waves 1, 2, and 13 through 19. The effect of wave height is to increase the phase velocity by about the same percentage for all the waves in the wave group, since the  $H_i/h_i$  ratio has a narrow variation in the inner surf zone. However, it is the longitudinal velocity of the long waves that has the biggest effect on the variation of phase velocity. Fig. 8 shows that  $C_4$  has a wide variation at all three locations near the shoreline. For example, the value of  $C_4$  at  $d=6.25$  cm is 1.29 m/s for wave 5 and 0.56 m/s for wave 11. The wave period changes as the position of the individual waves is changed relative to its neighbors. The changes in wave period are most noticeable for waves 1 and 10. Between  $d=18.23$  and  $6.25$  cm, the period for wave 1 has decreased by 33%, from 1.89 to 1.25 s, while the period for wave 10 has increased by 28%, from 2.58 to 3.31 s.

### 3.2. Turbulent kinetic energy and Reynolds stress

At  $d=13.72$ ,  $9.39$  and  $6.25$  cm, organized wave-induced velocity was obtained by ensemble averaging at five measurement points (see Table 1). The organized wave-induced velocity at other measurement points was estimated from these five ensemble-averaged velocity time series, assuming that the longitudinal velocity profile is uniform and the vertical velocity varies linearly with distance from the bottom.

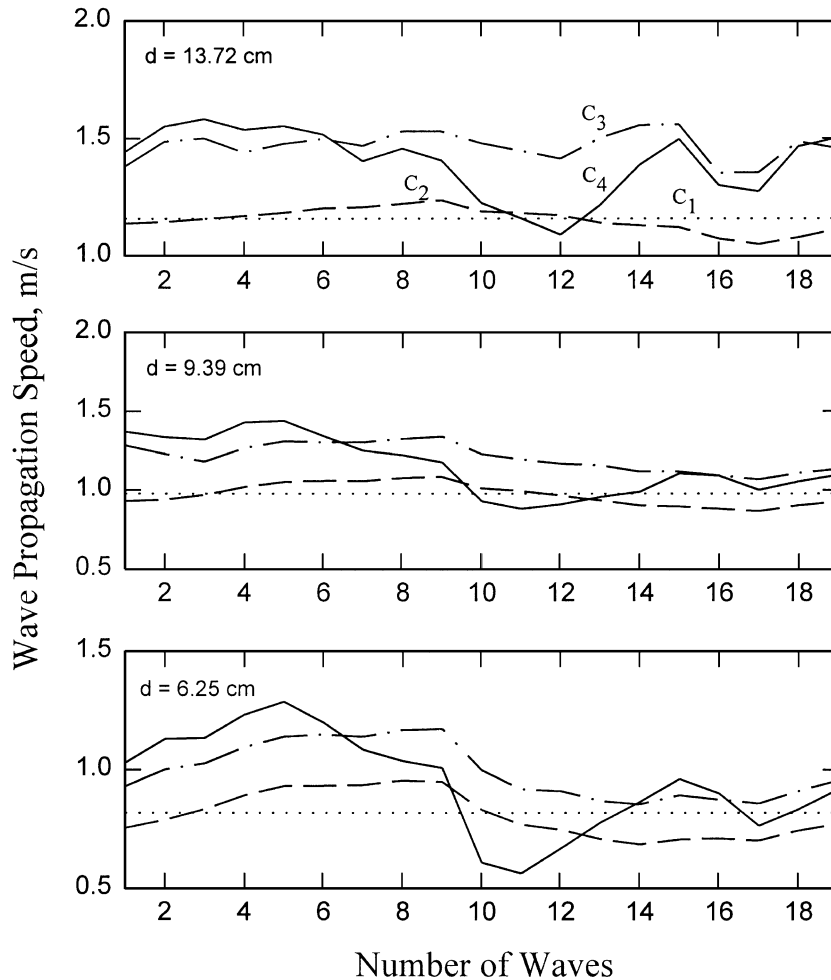


Fig. 8. Computed wave propagation speeds for the individual waves in wave group 4;  $C_1=(gh)^{1/2}$ ,  $C_2=(gh_i)^{1/2}$ ,  $C_3=[gh_i(1+H_i/h_i)]^{1/2}$  and  $C_4=[gh_i(1+H_i/h_i)]^{1/2}+U_i$ .

The difference between the measured instantaneous velocity and the organized wave-induced velocity is defined as the turbulent velocity fluctuation. This method is found to produce acceptable results for the time-averaged turbulent kinetic energy when compared with the ensemble averaging procedure (Ting, 2001).

Fig. 9 presents the profiles of the normalized time-averaged turbulent kinetic energy,  $[\bar{k}/(gh)]^{1/2}$ , at three cross-shore positions near the shoreline. Because the transverse velocity was not measured, the instantaneous turbulent kinetic energy  $k'$  is defined as  $1/2(u'^2+w'^2)$ , where  $u'$  and  $w'$  are the

longitudinal and vertical components of the turbulence velocity, respectively. Also shown in Fig. 9 are the turbulence measurements from a spilling regular wave (Ting and Kirby, 1994). That experiment was also conducted on a 1/35 plane slope. The deep-water wave height and wave length of the regular wave were 0.127 and 6.35 m, respectively, and the corresponding value of the surf similarity parameter was 0.20.

In the outer surf zone, the time-averaged turbulent kinetic energy for the narrow-band waves is similar in vertical structure but lower in magnitude than that for the spilling regular wave. In the inner surf zone, the

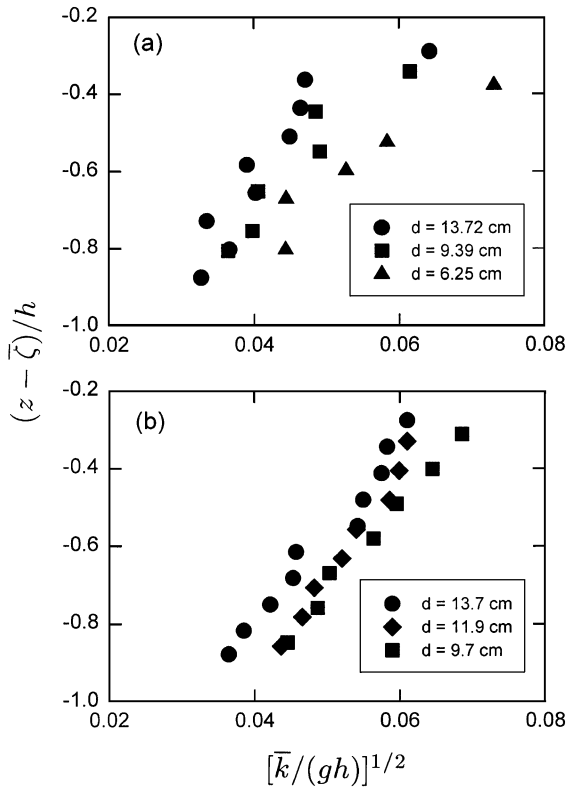


Fig. 9. Vertical distributions of time-averaged turbulent kinetic energy; (a) present experiment, and (b) Ting and Kirby (1994). The still water elevation is at  $z=0$ .

profiles of  $[\bar{k}/(gh)]^{1/2}$  under the regular and irregular waves are more similar. The turbulence measurements from the inner surf zone are consistent with the wave height measurements. For the regular spilling wave, the wave-height-to-water-depth ratio increases to a maximum value of 0.82 at the breaking point, and then decreases steadily to a constant value of 0.5 in the inner surf zone (Ting and Kirby, 1994). For the narrow-band waves, the  $H_i/h_i$  ratio varies from 0.7 to 1.1 at breaking, and from 0.5 to 0.6 at  $d=6.25$  cm (Fig. 4). Hence, the narrow-band waves and the spilling regular wave have similar wave-height-to-water-depth ratios in the inner surf zone.

Fig. 10 is a plot of the period-averaged turbulent kinetic energy time histories from the narrow-band waves. The measurements shown were taken at two different depths below the still water level  $z=0$ . The period average,  $k$ , was obtained by averaging the ensemble-averaged turbulent kinetic energy  $\langle k \rangle$  over

the wave period for the individual short waves. Comparing the plot for  $d=13.72$  cm in Fig. 10 with the plot for  $d=45.72$  cm in Fig. 4, it may be observed that in the outer surf zone, most of the turbulence energy is found under the waves with the larger initial heights, which are the first waves to break. The individual values of  $k$  were arranged in descending order until one third of the total number of waves was reached. The mean of the highest one-third values of  $k$  was calculated and denoted by  $k_{1/3}$ . Similarly, the mean of the  $k$  values of all the waves in the record was calculated and denoted by  $k_1$ . At  $d=13.72$  cm, the ratio  $(k_{1/3}/k_1)^{1/2}$  is 1.80 at  $(z-\bar{\zeta})/h=-0.363$  and 1.67 at  $(z-\bar{\zeta})/h=-0.728$ . At  $d=9.39$  cm, the ratio is 1.42 at  $(z-\bar{\zeta})/h=-0.446$  and 1.40 at  $(z-\bar{\zeta})/h=-0.651$ . At  $d=6.25$  cm, the last measuring position near the shoreline, the ratio is 1.25 at  $(z-\bar{\zeta})/h=-0.671$ . As seen, the range of  $k$  decreases as the still water depth decreases.

Fig. 11 is a plot of the period-averaged Reynolds stress correlation coefficient time histories. The Reynolds stress coefficient  $\tau$  is defined as  $\langle -u'w' \rangle / (\langle u'^2 \rangle \langle w'^2 \rangle)^{1/2}$ , where  $\langle \rangle$  denotes an operator to take an ensemble average. At  $d=13.72$  cm, the mean value of  $\tau$  is 0.11 at  $(z-\bar{\zeta})/h=-0.363$  and 0.10 at  $(z-\bar{\zeta})/h=-0.728$ . At  $d=9.39$  cm, the mean is 0.16 at  $(z-\bar{\zeta})/h=-0.446$  and 0.13 at  $(z-\bar{\zeta})/h=-0.651$ . At  $d=6.25$  cm, the mean is 0.17 at  $(z-\bar{\zeta})/h=-0.671$ . The standard deviation of  $\tau$  at these locations are 0.15, 0.12, 0.14, 0.12 and 0.11, respectively. The value of  $\tau$  is generally smaller at the lower level than at the upper level, consistent with the idea that the free surface layer is the source of most of the turbulence energy in breaking waves. Note that the mean value of  $\tau$  increases while the standard deviation decreases as the still water depth decreases.

A basic question is how the turbulent flow field under irregular breaking waves differs from that under regular breaking waves. Random wave breaking (in time and space) and low-frequency waves may change the dynamics of turbulence such that the turbulent flow field under irregular breaking waves is structurally different from that under regular breaking waves. The basic index of structure of turbulent motion is the ratios of the components of the Reynolds stress tensor. These ratios are different in different classes of turbulent flows such as free turbulent flows and boundary-layer flows (Townsend, 1976). The meas-

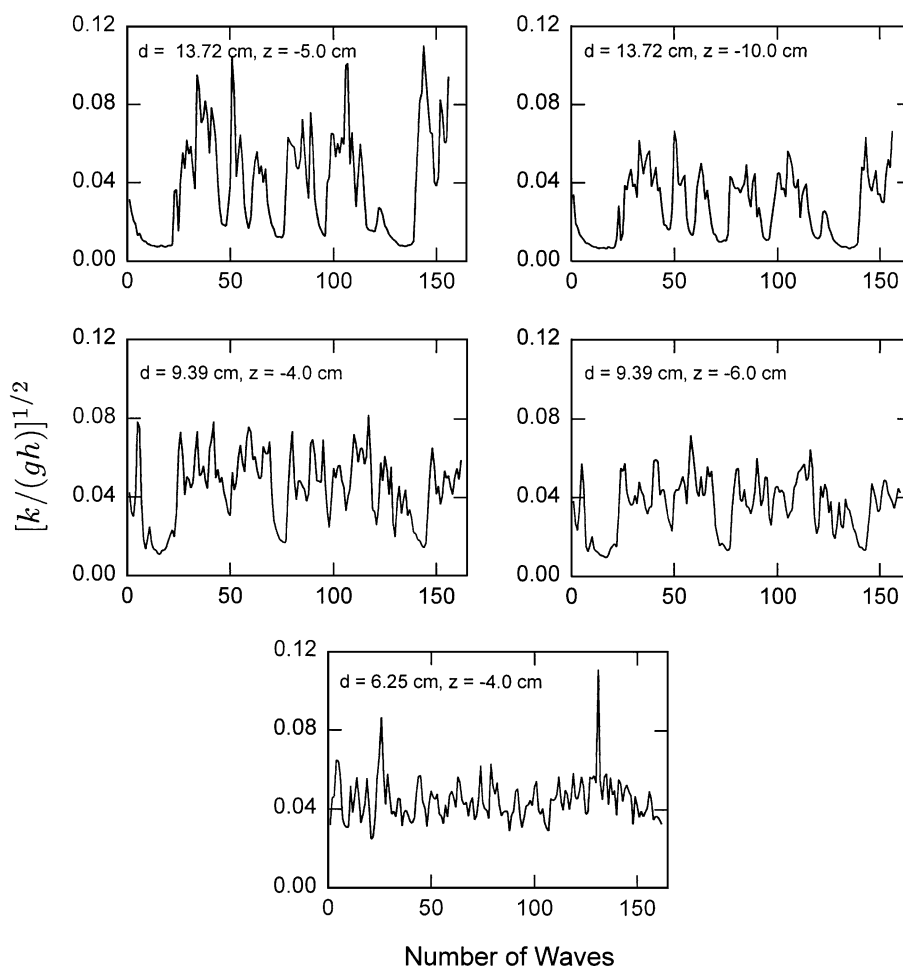


Fig. 10. Wave-averaged turbulent kinetic energy time histories.

measurements available do not permit a direct comparison of the Reynolds stress ratios in regular and irregular waves. Instead, the distribution of turbulent kinetic energy for the individual waves in a wave group is compared with similar measurements in regular waves (Ting and Kirby, 1995, 1996). Typical results are presented in Figs. 12–15.

In regular waves, there exists a similarity region in the inner surf zone where the turbulent kinetic energy at different vertical cross sections is similar when normalized by the local phase velocity (e.g. Ting and Kirby, 1996; Lin and Liu, 1998a,b). Fig. 12 shows the phase-averaged water surface elevation and turbulent kinetic energy time histories from a

spilling and a plunging regular wave. As shown in Fig. 12, the spilling wave and the plunging wave develop very different wave profiles and turbulent flow fields in the inner surf zone. In particular, the wave-height-to-water-depth ratio and turbulence intensity are much larger for the plunging wave. Under the plunging breaker, the temporal variation of turbulent kinetic energy is closely correlated to the wave profile, which indicates that the vertical mixing is strong; and most of the turbulent kinetic energy is dissipated within one wave cycle, which indicates that the time scale of turbulence is small compared with the wave period. Under the spilling breaker, a phase lag between the wave profile and the turbulent kinetic

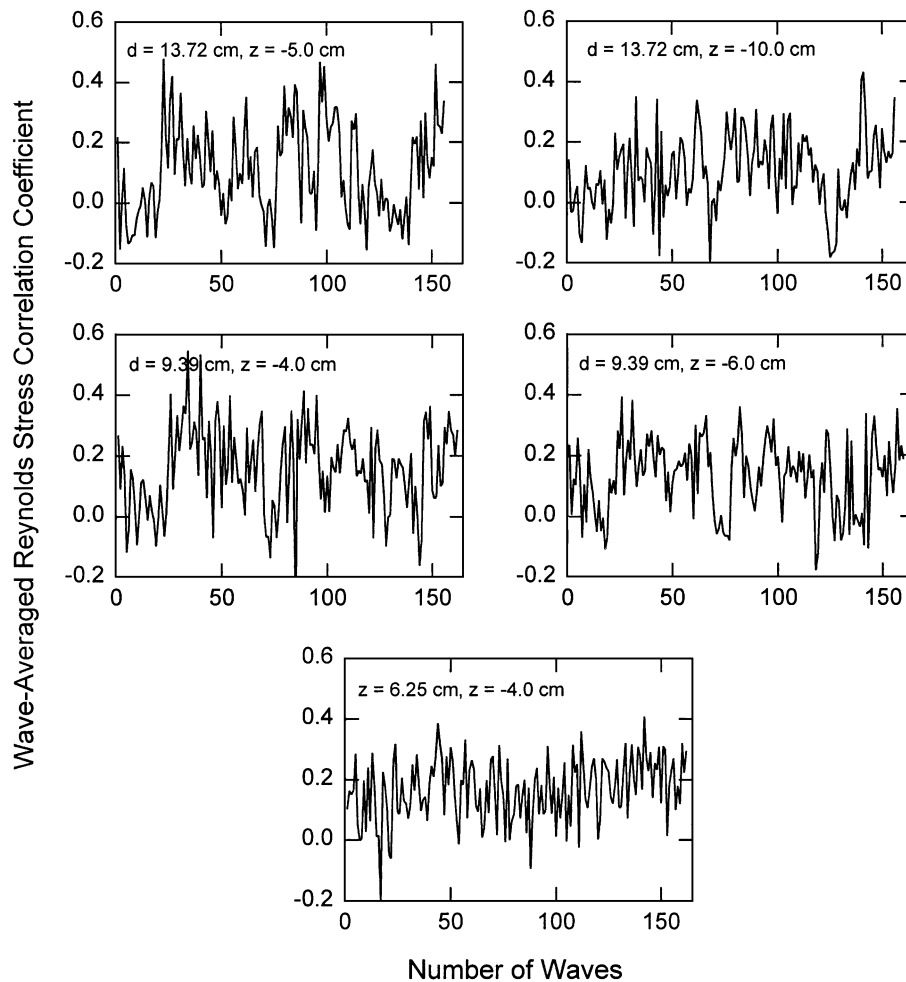


Fig. 11. Wave-averaged Reynolds stress correlation coefficient time histories.

energy increases with distance from the water surface. Furthermore, the temporal variation of turbulent kinetic energy over one wave cycle is small at the lower level. Fig. 12 shows that the turbulent flow field in the inner surf zone depends on a particular wave condition and it is not similar for different incident wave conditions. For irregular waves, this means that the flow field in the inner surf zone may vary considerably from wave to wave, depending on the wave height and wave period distributions in the incident waves.

Figs. 13–15 present the variations of  $\zeta_s/h_i$  and  $[\langle k_i \rangle / (gh_i)]^{1/2}$  with time at  $d = 13.72$ ,  $9.39$  and  $6.25$  cm (a, b and c) for waves 6, 5 and 15. The wave

characteristics for waves 6, 5 and 15, as well as those for the spilling regular wave and plunging regular wave, are presented in Table 3. The initial wave periods for waves 6, 5 and 15 are very close, but their deep-water wave heights are significantly different. Wave 6, which has the largest wave-height-to-wave-length ratio in deep water ( $H_0/L_0 = 0.0251$ ), breaks first, followed by wave 5 ( $H_0/L_0 = 0.0218$ ) and then wave 15 ( $H_0/L_0 = 0.0129$ ). All three waves developed into spilling breakers. Note that wave 5 and the spilling regular wave have similar  $H_0/L_0$  values.

Wave 6 breaks just after passing  $d = 22.77$  cm. The  $H_i/h_i$  ratios for wave 6 at  $d = 22.77$ ,  $18.23$ ,  $13.72$ ,  $9.39$  and  $6.25$  cm are  $0.812$ ,  $0.619$ ,  $0.551$ ,  $0.510$  and  $0.518$ ,

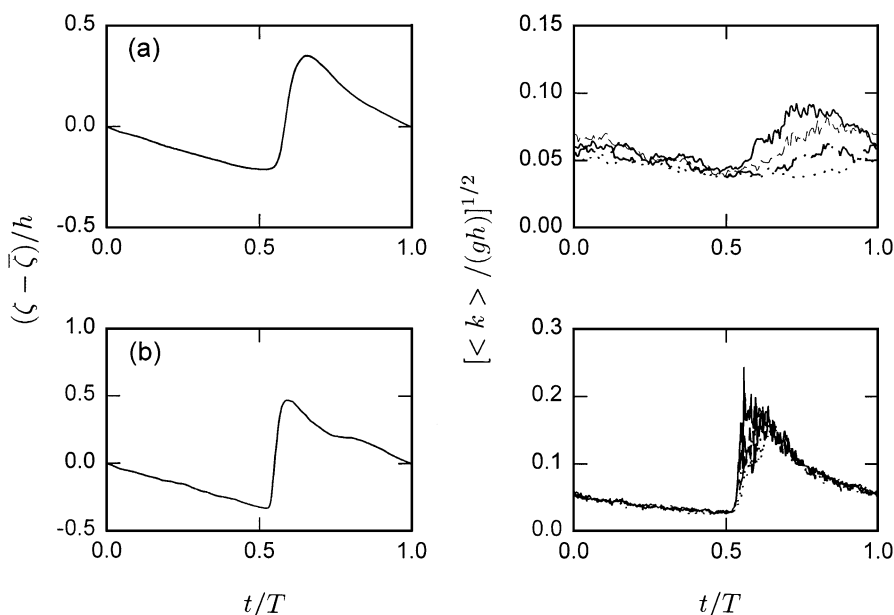


Fig. 12. Phase-averaged water surface elevation and turbulent kinetic energy time histories for (a) a spilling and (b) a plunging regular wave. The measurements in (a) were taken at  $(x - x_b)/h_b = 16.709$  and  $(z - \bar{\zeta})/h = -0.388$  (—),  $-0.477$  (- - -),  $-0.655$  (- · - ·) and  $-0.834$  (· · · ·). The measurements in (b) were taken at  $(x - x_b)/h_b = 16.883$  and  $(z - \bar{\zeta})/h = -0.456$  (—),  $-0.567$  (- - -),  $-0.678$  (- · - ·) and  $-0.861$  (· · · ·).

respectively. As shown in Fig. 13, the surface elevation and turbulent kinetic energy time histories at  $d = 9.39$  and  $6.25$  cm (b and c) are very close, which indicates that the broken wave has reached an equilibrium condition at these locations. The wave period for wave 6 increases as the still water depth decreases. The measured wave periods at  $d = 22.77$ ,  $18.23$ ,  $13.72$ ,  $9.39$  and  $6.25$  cm are  $2.06$ ,  $2.10$ ,  $2.12$ ,  $2.31$  and  $2.41$  s, respectively. Comparing Fig. 13 with Fig. 12, it is seen that the wave profile and the variation of turbulent kinetic energy with time from the irregular wave are similar to the those from the spilling regular wave.

Wave 5 starts breaking around  $d = 18.23$  cm. The  $H_i/h_i$  ratios at  $d = 18.23$ ,  $13.72$ ,  $9.39$  and  $6.25$  cm are  $0.915$ ,  $0.557$ ,  $0.549$  and  $0.499$ , respectively. As shown in Fig. 14, the wave profile for wave 5 is still evolving at  $d = 9.39$  cm (b). Comparing Fig. 14 with Fig. 13, the wave profile at  $d = 6.25$  cm (c) is similar for waves 5 and 6, while the turbulent kinetic energy is slightly larger under the wave crest for wave 5. The wave period for wave 5 decreases with the still water depth until  $d = 13.72$  cm and then increases. The measured periods at  $d = 18.23$ ,  $13.72$ ,  $9.39$  and  $6.25$  cm are  $1.74$ ,

$1.69$ ,  $1.70$  and  $1.77$  s, respectively. Comparing Fig. 14 with Fig. 12, the variation of turbulent kinetic energy with time under the wave crest is similar for the regular and irregular waves.

Wave 15 breaks at  $d = 13.72$  cm. The  $H_i/h_i$  ratios at  $d = 13.72$ ,  $9.29$  and  $6.25$  cm are  $0.928$ ,  $0.560$  and  $0.594$ , respectively. The wave period for wave 15 fluctuates as the wave propagates through the surf zone. The measured periods at  $d = 13.72$ ,  $9.39$  and  $6.25$  cm are  $2.45$ ,  $2.11$  and  $1.75$  s, respectively. As the  $H_0/L_0$  value decreases, the breaker type gradually changes from spilling toward plunging. Fig. 15 shows that the temporal variation of  $[\langle k_i \rangle / (gh_i)]^{1/2}$  is larger for wave 15 than for waves 6 and 5, which is consistent with the smaller  $H_0/L_0$  value for wave 15. Comparing Fig. 15 with Fig. 12, the flow field is more turbulent for wave 15 than for the spilling regular wave, but less turbulent for wave 15 than for the plunging regular wave.

The  $H_i/h_i$  ratio at breaking was computed using the empirical formula of Hansen (1990). This formula was derived from experimental data on regular waves obtained by Hansen and Svendsen (1979). As shown in Table 3, the predicted and measured  $H_i/h_i$  ratios are

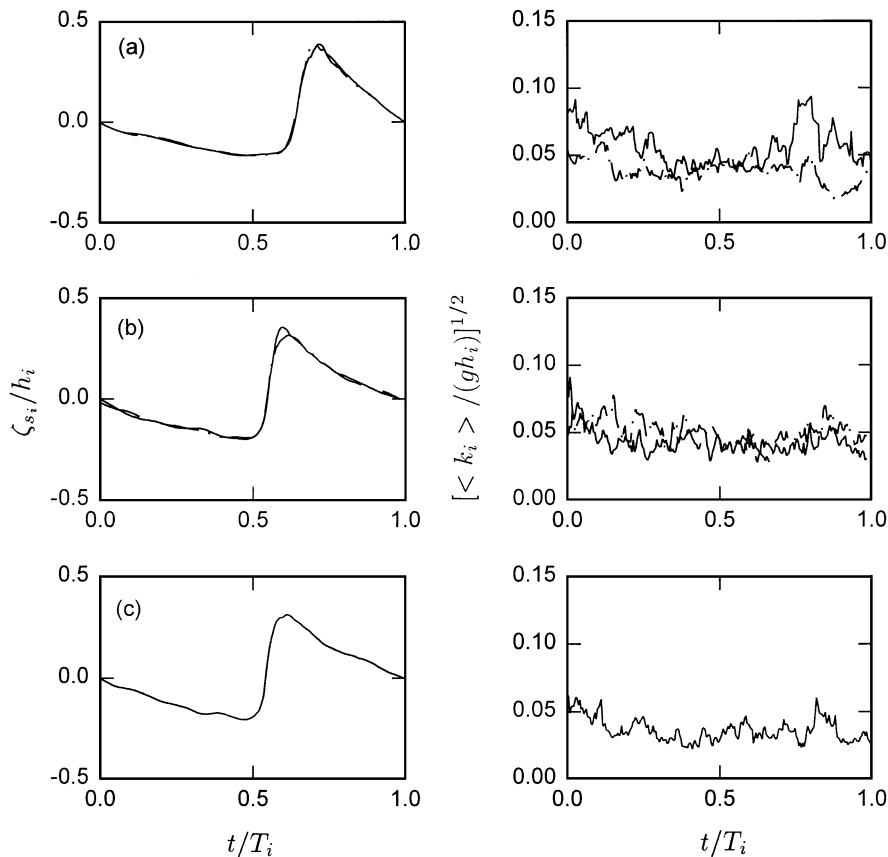


Fig. 13. Ensemble-averaged water surface elevation and turbulent kinetic energy time histories for wave 6. (a)  $(x - x_b)/h_b = 13.60$  and  $(z - \bar{\zeta}_i)/h_i = -0.411$  (—) and  $-0.748$  (---); (b)  $(x - x_b)/h_b = 20.21$  and  $(z - \bar{\zeta}_i)/h_i = -0.530$  (—) and  $-0.704$  (---); (c)  $(x - x_b)/h_b = 24.82$  and  $(z - \bar{\zeta}_i)/h_i = -0.746$  (—).

reasonably close. For wave breaking in periodic wave groups, Svendsen and Veeramony (2001) showed that the  $H/h$  ratio at breaking has a wider variation for the individual waves in a wave group than for monochromatic waves. This may be expected since random wave breaking (in space and time) and low-frequency waves create a constantly changing environment for the breaking waves. However, the present study shows no evidence that the distribution of turbulent kinetic energy in the inner surf zone is substantially different in narrow-band waves and regular waves if the waves have the same surf similarity parameter value.

The correlation between the organized wave-induced velocity and turbulence intensity may be an important factor for sediment transport in the coastal

zone. Ting and Kirby (1994) observed that the time-averaged transport of turbulent kinetic energy by the ensemble-averaged velocity is seaward under a spilling regular wave and landward under a plunging regular wave. Fig. 16 presents the time-averaged cross-shore transport of turbulent kinetic energy under the narrow-band waves. Transport of turbulent kinetic energy by turbulence velocity  $u'$  is defined as  $\langle k'u' \rangle$ . Transport of turbulent kinetic energy by the short-wave velocity  $u$ , long-wave velocity  $U$  and the undertow  $\bar{u}$  are defined as  $\langle k'u \rangle$ ,  $\langle k'U \rangle$  and  $\langle k'\bar{u} \rangle$ , respectively.

As shown in Fig. 16, the short waves and the breaker-generated turbulence transport turbulent kinetic energy landward, while the undertow transports turbulent kinetic energy seaward. The cross-

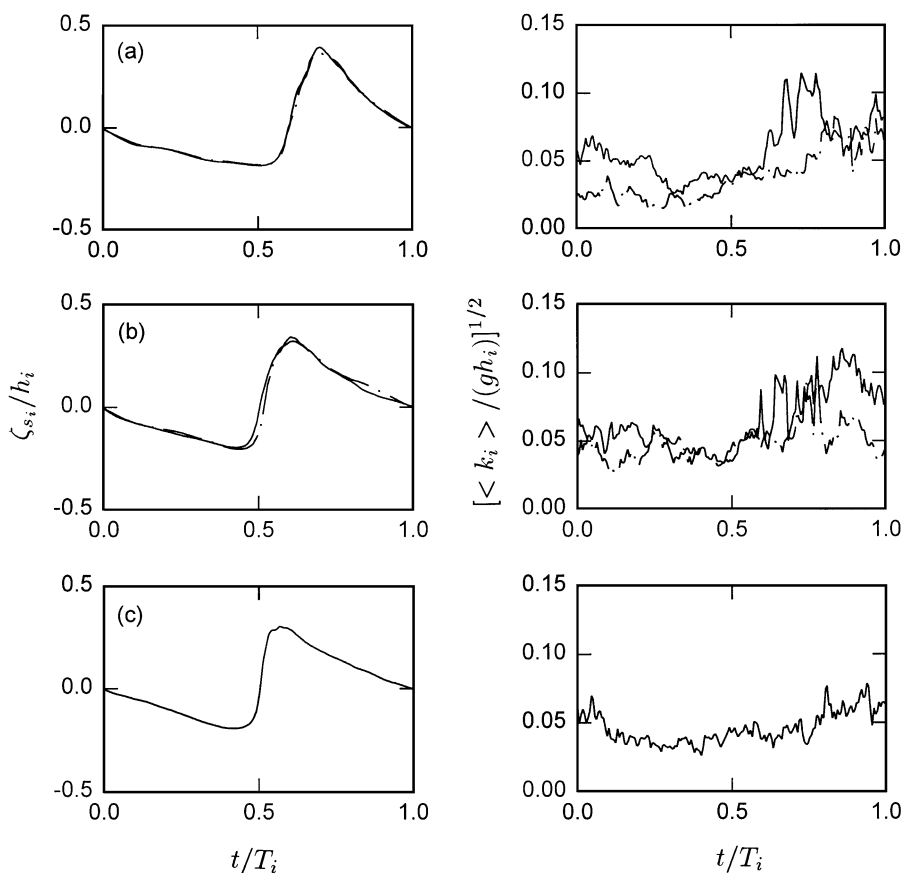


Fig. 14. Ensemble-averaged water surface elevation and turbulent kinetic energy time histories for wave 5. (a)  $(x - x_b)/h_b = 8.57$  and  $(z - \bar{\zeta}_i)/h_i = -0.392$  (—) and  $-0.740$  (---); (b)  $(x - x_b)/h_b = 16.96$  and  $(z - \bar{\zeta}_i)/h_i = -0.524$  (—) and  $-0.701$  (---); (c)  $(x - x_b)/h_b = 22.79$  and  $(z - \bar{\zeta}_i)/h_i = -0.746$  (—).

shore transport of turbulent kinetic energy by the short-wave velocity decreases with distance from the water surface, due to decrease in turbulence intensity and increase in the phase lag between the horizontal velocity and turbulent kinetic energy from the surface downward. The long-wave motion can transport turbulent kinetic energy onshore or offshore, depending on the location inside the surf zone. However, since the long waves were generated by wave breaking and re-reflected from the wave maker, the turbulence transport by the long waves in the wave tank may be different from that on a natural beach. Nevertheless, these results indicate that in a surf zone with predominately spilling breakers, the transport of turbulent kinetic energy is seaward in the

lower layer and it is dominated by the undertow. Similar results were observed in broad-band waves (Ting, 2001).

### 3.3. Comparisons with broad-band waves

Using the same experimental arrangement, Ting (2001) measured the wave elevation and water particle velocity inside the surf zone created by the breaking of a broad-band irregular wave train. The broad-band waves have measured  $H_{1/3}$  and  $T_{1/3}$  of 13.32 cm and 1.74 s at  $d = 45.72$  cm. The corresponding values of  $H_0$ ,  $H_0/L_0$  and  $\xi_0$  are 14.24 cm, 0.0301 and 0.165, respectively, whereas the narrow-band waves have measured  $H_{1/3}$  and  $T_{1/3}$  of 12.16 cm and

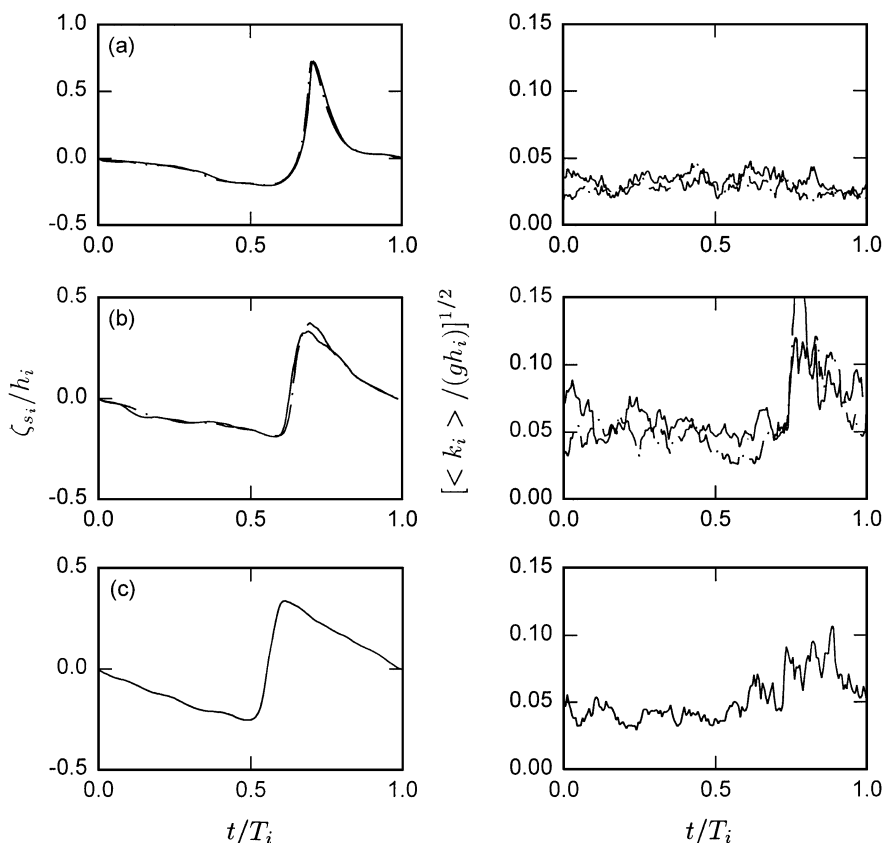


Fig. 15. Ensemble-averaged water surface elevation and turbulent kinetic energy time histories for wave 15. (a)  $(x-x_b)/h_b=0.0$  and  $(z-\zeta_i)/h_i=-0.323$  (—) and  $-0.711$  (---); (b)  $(x-x_b)/h_b=11.16$  and  $(z-\zeta_i)/h_i=-0.342$  (—) and  $-0.587$  (---); (c)  $(x-x_b)/h_b=18.93$  and  $(z-\zeta_i)/h_i=-0.559$  (—).

1.98 s at  $d=45.72$  cm, and the corresponding values of  $H_0$ ,  $H_0/L_0$  and  $\xi_0$  are 12.63 cm, 0.0207 and 0.199, respectively. The measured wave spectra for the narrow-band waves and broad-band waves are presented in Fig. 2.

Fig. 17 presents the measured  $H_i/h_i$  ratio for the broad-band waves. Comparing Fig. 17 with Fig. 4, the variations of the  $H_i/h_i$  ratio are more random for the broad-band waves. In Fig. 17, the maximum values of  $H_i/h_i$  at  $d=45.72, 27.04, 22.77, 18.23, 13.72, 9.39$  and  $6.25$  cm are 0.433, 0.718, 0.811, 0.875, 0.829, 1.052 and 1.119, respectively. Except for  $d=13.72$  cm, the maximum value of  $H_i/h_i$  increases as the still water depth decreases. These results indicate that the waves that break closer to shore generally have larger  $H_i/h_i$  ratios at breaking than the waves that break farther

offshore. After breaking, the  $H_i/h_i$  ratio decreases with the still water depth. The mean value of  $H_i/h_i$  at  $d=6.25$  cm is 0.502. As in the narrow-band waves, normalizing the individual wave height by the period-averaged water depth greatly reduces the variation in the  $H_i/h_i$  ratio. Hence, the time-varying water depth associated with the long-wave motion is an important factor in the wave transformation through the surf zone.

Comparing Fig. 17 with Fig. 4, it may be observed that the broad-band waves have a wider variation in the  $H_i/h_i$  ratio at  $d=6.25$  cm. In both figures, the large  $H_i/h_i$  values are from waves that are near their breaking points, and the small  $H_i/h_i$  values are from secondary waves in the wave profiles that are interpreted as individual waves by the zero-downcrossing

Table 3  
Wave characteristics for waves 5, 6 and 15, spilling regular wave (S), and plunging regular wave (P)

Wave	5	6	15	S	P
$T$ (s)	1.90	1.96	2.02	2.0	5.0
$H_0$ (cm)	12.30	15.05	8.21	12.70	8.90
$H_0/L_0$	0.0218	0.0251	0.0129	0.0204	0.0023
$\zeta_0$	0.19	0.18	0.25	0.20	0.60
$H_b$ (cm)	17.1	18.8	11.9	16.3	18.4
$h_b$ (cm)	18.7	23.1	12.9	19.9	15.4
$(H/h)_b$ , measured	0.92	0.81	0.93	0.82	1.20
$(H/h)_b$ , predicted	0.90	0.89	0.94	0.90	1.10

$T$ =wave period measured in the horizontal portion of the wave tank;  $H_0$ =deep-water wave height;  $L_0$ =deep-water wave length;  $\zeta_0$ =surf similarity parameter;  $H_b$ =breaker height;  $h_b$ =breaking depth.

method. Figs. 4 and 17 show that there are more broad-band waves than narrow-band waves that did not reach a depth-limited condition at  $d=6.25$  cm. These results are consistent with the observation that a high percentage of wave breaking occurred near the shoreline in the case of the broad-band waves.

Figs. 4 and 17 show that the number of waves decreases inside the surf zone for the broad-band waves but remains about the same for the narrow-band waves. The distributions of wave height and phase velocity are more random in the broad-band waves. It was observed that many small waves were overtaken and absorbed by following large waves that were moving faster. For the narrow-band waves, a high level of groupiness in the incident waves means that adjacent waves often have similar wave characteristics such as wave-height-to-water-depth ratio and phase velocity. This may be the reason why fewer narrow-band waves were captured by their neighbors.

Fig. 18 presents the probability distributions of  $[k/(gh)]^{1/2}$  from the narrow-band waves and broad-band waves. The distribution of  $[k/(gh)]^{1/2}$  from the narrow-band waves shows that not all the waves are turbulent in the outer surf zone. At  $d=13.72$  cm, non-breaking waves are found at the head and rear of the wave groups. These are the waves with the smaller initial heights. Since adjacent groups of breaking waves are separated in between by non-breaking waves, the distribution of  $[k/(gh)]^{1/2}$  has a large standard deviation. Most of the waves have broken at  $d=6.25$  cm,

and thus  $[k/(gh)]^{1/2}$  has a narrow variation. Compared to the narrow-band waves, the broad-band waves has a smaller range of  $[k/(gh)]^{1/2}$  values at  $d=13.72$  cm. This is because wave breaking is more random for the broad-band waves. The turbulence generated by one breaker does not die out completely before the arrival of the next breaker. Hence, the turbulent kinetic energy generated by wave breaking is more uniformly distributed among the breaking and non-breaking waves.

Comparing the distributions of  $[k/(gh)]^{1/2}$  at  $d=6.25$  cm from the narrow-band waves and the broad-band waves, the results show that changing the shape of the incident wave spectrum does not affect the distribution of the wave-averaged turbulent kinetic energy greatly in the inner surf zone, while the experimental data from Sultan (1995) suggest that

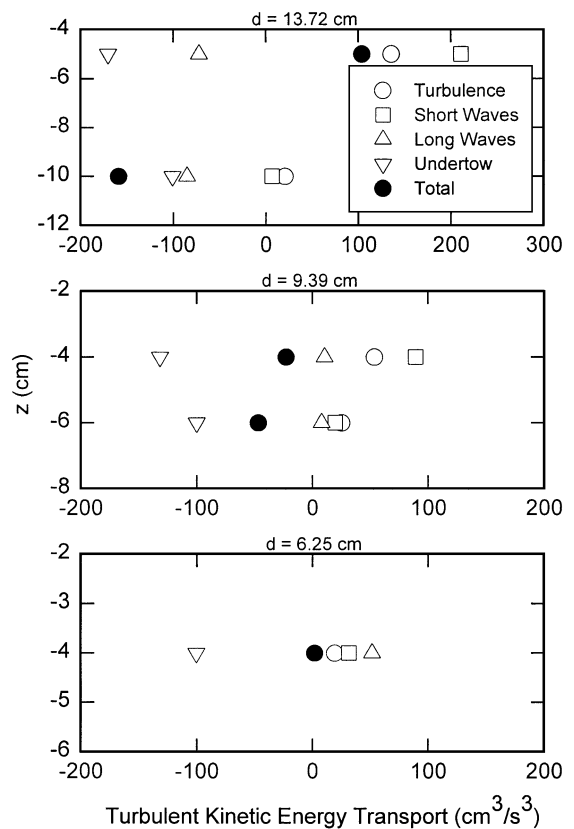


Fig. 16. Time-averaged transport of turbulent kinetic energy in the onshore/offshore direction by turbulence, short-wave velocity, long-wave velocity, and undertow.

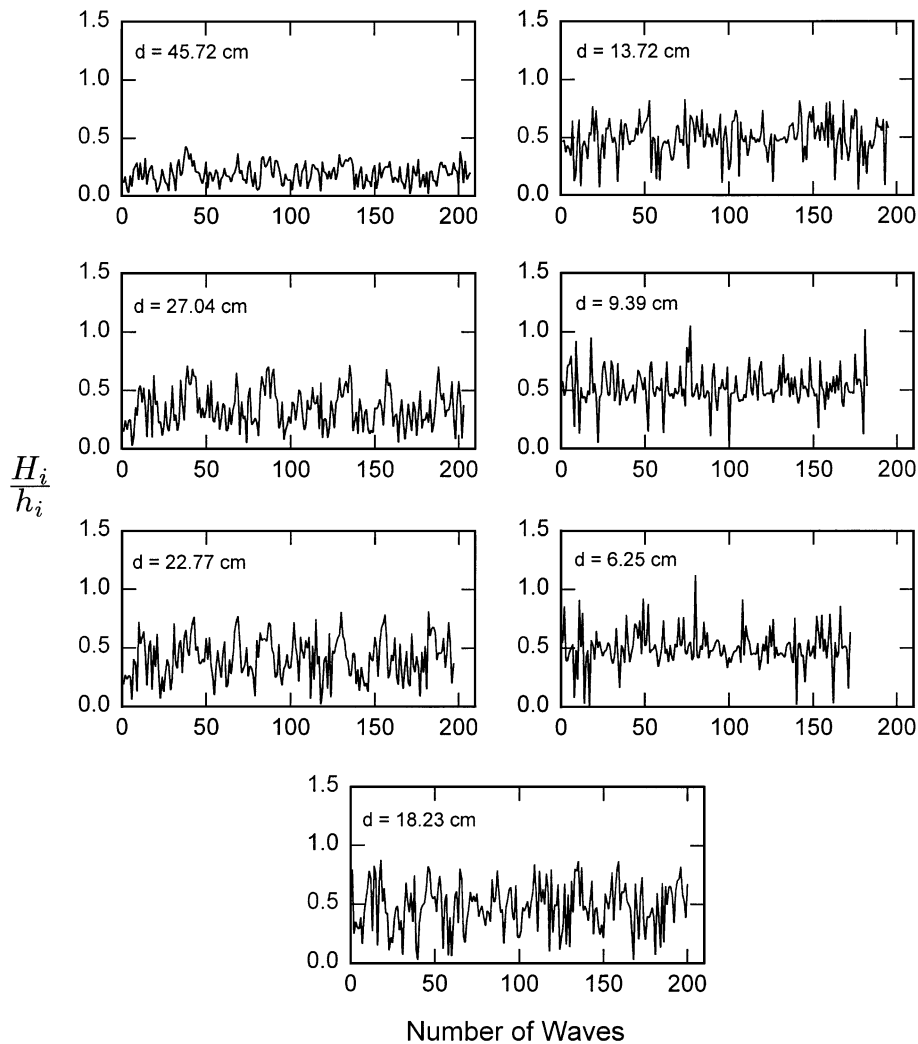


Fig. 17. Wave-height-to-water-depth ratio for broad-band waves.

other parameters such as the significant wave height and wave period of the incident waves are more important in determining the structure of turbulence under breaking waves. Laboratory studies on a spilling and a plunging regular wave have shown that the turbulent flow field in the inner surf zone depends on a particular breaker type, and it is not similar for different breaker types (Fig. 12). For regular waves, the breaker type is characterized by the surf similarity parameter  $\xi_0$ . When  $H_0$  and  $L_0$  are calculated by backing the measured  $H_{1/3}$  and  $T_{1/3}$  from the horizontal portion of the wave tank to deep water,  $\xi_0$  has a

value of 0.199 for the narrow-band waves and 0.165 for the broad-band waves. For both wave conditions, the surf zone is dominated by spilling type breakers. It is suggested that the distribution of turbulent kinetic energy in the inner surf zone is primarily determined by the breaker types. The narrow-band and broad-band waves have similar distributions of  $[k/(gh)]^{1/2}$  in the inner surf zone because their wave characteristics in the inner surf zone are similar and the turbulence is produced by similar breaker types. On the other hand, significant differences in the distribution of  $[k/(gh)]^{1/2}$  are found between the

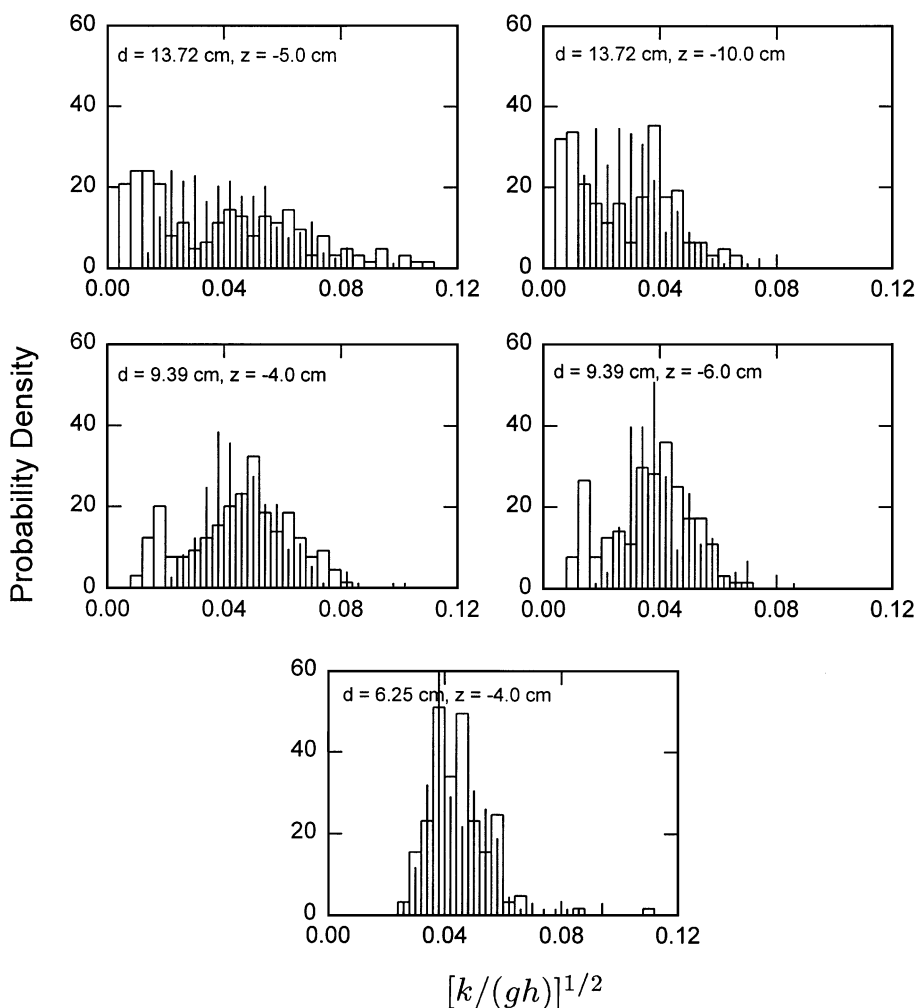


Fig. 18. Probability density of wave-averaged turbulent kinetic energy for narrow-band waves (wide bar) and broad-band waves (narrow bar).

narrow-band waves and broad-band waves in the outer surf zone. The observed differences are related to the temporal and spatial variability of wave breaking, which is strongly dependent on the shape of the incident wave spectrum.

#### 4. Conclusions

The main conclusions that can be drawn from this investigation are stated below.

(1) Even through the surf zone, the narrow-band waves form wave groups that are strongly modulated.

The order in which the individual waves break follows closely their initial heights in the groups. In general, the waves that break close to shore have larger wave-height-to-water-depth ratios prior to breaking than the waves that break farther offshore. The wave-height-to-water-depth ratio for the individual waves approaches a constant value in the inner surf zone.

(2) The long waves generated by wave breaking alter the local water depth and create a time-varying current, which have a significant effect on the short waves riding on them. The wave period is found to have a wider variation inside the surf zone than the

incident waves. The transformation of wave period is related to variations in phase velocity of the waves in the wave groups.

(3) Close to shore, the wave-height-to-water-depth ratio is found to have a wider variation for broad-band waves than for narrow-band waves.

(4) The number of waves decreases through the surf zone for the broad-band waves, but remains about the same for the narrow-band waves. The capturing of slow moving, small waves by fast moving, large waves was frequently observed in the broad-band waves but not in the narrow-band waves.

(5) A wave-by-wave analysis for the individual waves in a wave group shows that the ensemble-averaged water surface elevation and turbulent kinetic energy time histories in the inner surf zone are qualitatively similar to the measurements from a spilling regular wave that has similar  $\xi_0$  value as the irregular waves. The vertical distribution of the time-averaged turbulent kinetic energy in the inner surf zone is also similar for the narrow-band waves and the spilling regular wave.

(6) Inside the surf zone, the time-averaged transport of turbulent kinetic energy by the organized wave-induced flow is seaward in the lower layer and is dominated by the undertow. The cross-shore transport of turbulent kinetic energy in an irregular wave surf zone with predominantly spilling breakers is consistent with that found under a spilling regular wave.

(7) In the outer surf zone, the distribution of the period-averaged turbulent kinetic energy from the narrow-band waves is closely correlated to the initial wave heights of the waves in the wave groups, and has a wider variation for narrow-band waves than for broad-band waves. In the inner surf zone, the distribution of the period-averaged turbulent kinetic energy is similar for narrow-band waves and broad-band waves.

(8) The experimental results indicate that the shape of the incident wave spectrum has a significant effect on the temporal and spatial variability of wave breaking and the distribution of turbulent kinetic energy in the outer surf zone. In the inner surf zone, however, the wave-height-to-water-depth ratio and the distribution of turbulent kinetic energy are relatively insensitive to the shape of the incident wave spectrum. Other factors, such as the significant wave height and period of the incident waves, are found to be more important

in determining the wave and turbulence characteristics in the inner surf zone.

## Acknowledgements

This study was sponsored by the Office of Naval Research through Grant N00014-00-1-0461. Their support is gratefully acknowledged.

## References

- Battjes, J.A., 1974. Surf similarity. Proc. 14th Int. Coastal Eng. Conf., Copenhagen. ASCE, New York, pp. 466–480.
- Bouws, E., Gunther, H., Rosenthal, W., Vincent, C.L., 1985. Similarity of wind wave spectrum in finite depth water: Part 1. Spectral form. *J. Geophys. Res.* 90 (C1), 975–986.
- Bradford, S., 2000. Numerical simulation of surf zone dynamics. *J. Waterw. Port Coast. Ocean Eng.* 126, 1–13.
- Cox, D.T., Kobayashi, N., 2000. Identification of intense, intermittent coherent motions under shoaling and breaking waves. *J. Geophys. Res.* 105 (C6), 14223–14236.
- Cox, D.T., Kobayashi, N., Okayasu, A., 1996. Bottom shear stress in the surf zone. *J. Geophys. Res.* 101 (C6), 14337–14348.
- Dalrymple, R.A., 1992. Prediction of storm/normal beach profiles. *J. Waterw. Port Coast. Ocean Eng.* 118, 193–200.
- Dean, R.G., 1973. Heuristic model of sand transport in the surf zone. Proc. Engineering Dynamics in the Surf Zone. Institute of Engineers, Australia, pp. 208–214.
- Deigaard, R., Fredsøe, J., Hedegaard, I.B., 1986. Suspended sediment in the surf zone. *J. Waterw. Port Coast. Ocean Eng.* 112, 115–129.
- Galvin, C.J., 1968. Breaker type classification on three laboratory beaches. *J. Geophys. Res.* 73, 3651–3659.
- Goda, Y., 1970. A synthesis of breaker indices. *Trans. Jpn. Soc. Civ. Eng.* 2, 227–230.
- Hansen, J.B., 1990. Periodic waves in the surf zone: analysis of experimental data. *Coast. Eng.* 14, 19–41.
- Hansen, J.B., Svendsen, I.A., 1979. Regular waves in shoaling water, experimental data. *Inst. Hydrodyn. Hydraul. Eng., Technical Univ. Denmark, Ser. Pap.* 21.
- Lemos, C.M., 1992. Wave Breaking, a Numerical Study. Springer-Verlag, New York, 196 pp.
- Lin, P., Liu, P.L.-P., 1998a. A numerical study of breaking waves in the surf zone. *J. Fluid Mech.* 359, 239–264.
- Lin, P., Liu, P.L.-P., 1998b. Turbulence transport, vorticity dynamics, and solute mixing under plunging breaking waves in surf zone. *J. Geophys. Res.* 103 (C8), 15677–15694.
- Nadaoka, K., Kondoh, T., 1982. Laboratory measurements of velocity field structure in the surf zone by LDV. *Coast. Eng. Jpn.* 25, 125–146.
- Nadaoka, K., Hino, M., Koyano, Y., 1989. Structure of turbulent flow field under breaking waves in the surf zone. *J. Fluid Mech.* 204, 359–387.

- Okayasu, A., Shibayama, T., Nimura, N., 1986. Velocity field under plunging waves. Proc. 20th Int. Coastal Eng. Conf., Taipei. ASCE, New York, pp. 660–674.
- Stive, M.J.F., 1980. Velocity and pressure field of spilling breakers. Proc. 17th Int. Coastal Eng. Conf., Sydney. ASCE, New York, pp. 547–566.
- Stive, M.J.F., Wind, H.J., 1982. A study of radiation stress and set-up in the surf zone. *Coast. Eng.* 6, 1–25.
- Sultan, N.J., 1995. Irregular wave kinematics in the surf zone. PhD thesis, Department of Civil Engineering, Texas A and M University, College Station, TX, 135 pp.
- Sultan, N.J., Ting, F.C.K., 1993. Experimental study of undertow and turbulence intensity under irregular waves in the surf zone. Proc. 2nd Int. Symposium on Ocean Wave Measurement and Analysis, New Orleans. ASCE, New York, pp. 602–613.
- Svendsen, I.A., Veeramony, J., 2001. Wave breaking in wave groups. *J. Waterw. Port Coast. Ocean Eng.* 127, 200–212.
- Svendsen, I.A., Madsen, P.A., Hansen, J.B., 1978. Wave characteristics in the surf zone. Proc. 16th Int. Coastal Eng. Conf., Hamburg. ASCE, New York, pp. 520–539.
- Ting, F.C.K., 2001. Laboratory study of wave and turbulence velocities in a broad-banded irregular wave surf zone. *Coast. Eng.* 43, 183–208.
- Ting, F.C.K., Kirby, J.T., 1994. Observation of undertow and turbulence in a laboratory surf zone. *Coast. Eng.* 24, 51–80.
- Ting, F.C.K., Kirby, J.T., 1995. Dynamics of surf-zone turbulence in a strong plunging breaker. *Coast. Eng.* 24, 177–204.
- Ting, F.C.K., Kirby, J.T., 1996. Dynamics of surf-zone turbulence in a spilling breaker. *Coast. Eng.* 27, 131–160.
- Townsend, A.A., 1976. *The Structure of Turbulent Shear Flow*. Cambridge Univ. Press, Cambridge, 429 pp.